Bioorganic & Medicinal Chemistry Letters 30 (2020) 127510

Contents lists available at ScienceDirect

Bioorganic & Medicinal Chemistry Letters

journal homepage: www.elsevier.com/locate/bmcl

Fragment-based lead discovery of a novel class of small molecule antagonists of neuropeptide B/W receptor subtype 1 (GPR7)

Remond Moningka[a,*], F. Anthony Romero[a], Nicholas B. Hastings[b], Zhiqiang Guo[a], Ming Wang[a], Jerry Di Salvo[c], Ying Li[c], Dorina Trusca[c], Qiaoling Deng[d], Vincent Tong[e], Jenna L. Terebetski[f], Richard G. Ball[g], Feroze Ujjainwalla[a]

[a] Merck & Co., Inc., Department of Medicinal Chemistry, PO Box 2000, Rahway, NJ 07065, USA
[b] Merck & Co., Inc., Department of Neuroscience and Ophthalmology, Kenilworth, NJ 07033, USA
[c] Merck & Co., Inc., Department of In Vitro Pharmacology, PO Box 2000, Rahway, NJ 07065, USA
[d] Merck & Co., Inc., Department of Chemistry Modeling and Informatics, PO Box 2000, Rahway, NJ 07065, USA
[e] Merck & Co., Inc., Department of Pharmacokinetics, Pharmacodynamics, and Drug Metabolism, PO Box 2000, Rahway, NJ 07065, USA
[f] Merck & Co., Inc., Department of Basic Pharmaceutical Sciences, PO Box 2000, Rahway, NJ 07065, USA
[g] Merck & Co., Inc., Department of Analytical Chemistry, PO Box 2000, Rahway, NJ 07065, USA

ARTICLE INFO

Keywords:
NPBWR1
GPR7
Anti-obesity
G protein-coupled receptor
Schild plot analysis

ABSTRACT

Here, we report the discovery of a new class of NPBWR1 antagonists identified from a fragment-based screen. Compound **1** (cAMP IC_{50} = 250 μM; LE = 0.29) emerged as an initial hit. Further optimization of **1** by SAR-by-catalogue and chemical modification produced **21a** (cAMP IC_{50} = 30 nM; LE = 0.39) with a 6700-fold increase in potency from fragment **1**. Somewhat surprisingly, Schild analysis of compound **21a** suggested that in vitro inhibition of NPW-mediated effects on upon cAMP accumulation were saturable, and that compound **21a** dose-dependently increased [125I]-hNPW23 dissociation rate constants from NPBWR1 in kinetic binding studies. Collectively, these data are inconsistent with a classic surmountable, orthosteric mechanism of inhibition. The benzimidazole inhibitors reported herein may therefore represent a mechanistically differentiated class of compounds with which to form a better appreciation of the pharmacology and physiological roles of this central neuropeptide system.

Introduction

The G protein-coupled receptor 7 (GPR7) was deorphanized with the identification of endogeneous ligands neuropeptide B (NPB) and neuropeptide W (NPW)[1] and was reclassified as the neuropeptide B/W receptor-1 (NPBWR1). NPBWR1 is present in peripheral tissues, but is primarily expressed within the central nervous system (CNS) and widely distributed in the hippocampus, subcortical limbic telencephalon, hypothalamus, olfactory cortex, midbrain periaqueductal gray and tegmental area.[2]

Several studies have suggested that NPBWR1 has a role in regulating feeding behavior, energy homeostatis, neuroendocrine function, and modulating inflammatory pain.[3] Intracerebroventricular (i.c.v.) injection of NPW and NPB was shown to increase food intake and cause acute hyperphagia in male rats, respectively.[1b,d] Furthermore, NPBWR1 knockout mice developed an adult-onset obese phenotype that progressively worsened with age and was significantly exacerbated when animals were fed a high-fat diet.[4] Encouraged by these studies we sought to probe NPBWR1 as a potential novel anti-obesity target.

We have previously reported the development of a picomolar small molecule antagonist of NPBWR1 from a high-throughput screening hit in order to develop tools to study the physiological function of NPBWR1.[5] A distinct chemical series has also been developed from a group at The Scripps Research Institute culminating in CYM50769.[6] While these compounds represent potential tool compounds to interrogate NPBWR1, we had continued interest in developing novel chemical matter. Here we describe the fragment-based design and struc-

* Corresponding author.
E-mail address: remond_moningka@merck.com (R. Moningka).

https://doi.org/10.1016/j.bmcl.2020.127510
Received 2 June 2020; Received in revised form 14 August 2020; Accepted 17 August 2020
Available online 06 September 2020
0960-894X/

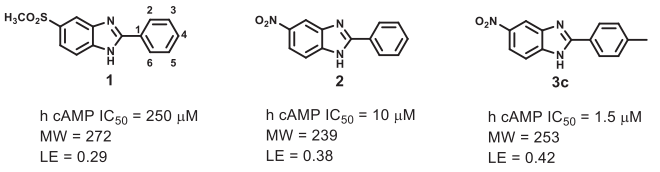

Fig. 1. In vitro potency of fragment hit **1**, SAR-by-catalogue hit **2** and analog **3** at NPBWR1.

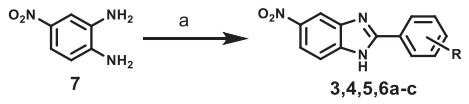

Scheme 1. Reagents and conditions: (a) *o*, *m*, *p*-substituted benzaldehyde, ammonium acetate, 75 °C.

Table 1
Effects of ortho, meta and para substituents on potency and LE.

cmpd	R		cAMP IC_{50} (nM)	LE
3	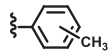	3a *ortho*	16940	0.34
		3b *meta*	31460	0.32
		3c *para*	1517	0.42
4		4a *ortho*	10680	0.36
		4b *meta*	9979	0.36
		4c *para*	2687	0.40
5	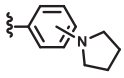	5a *ortho*	6770	0.31
		5b *meta*	6013	0.31
		5c *para*	1814	0.34
6	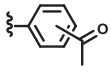	6a *ortho*	>31600	-
		6b *meta*	>31600	-
		6c *para*	9318	0.33

ture–activity relationship (SAR) studies of a negative allosteric modulator of NPBWR1.

Fragment-based drug discovery is now a routine technology to find novel chemical matter for drug discovery projects.[7] While an x-ray structure of the fragment bound to the protein often selects for fragment follow-up and provides a path for hypothesis-driven chemistry to develop the fragment hit, it is not necessarily required for fragment-based lead discovery. Biophysical methods also exist to drive fragment follow-up, such as surface plasmon resonance (SPR) and NMR. We developed a

Table 2
Exploration of the para position at the right-hand aryl group.

cmpd	R	cAMP IC_{50} (nM)	LE
3c		1500	0.42
4c	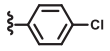	2687	0.40
8a	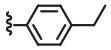	1016	0.41
8b	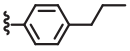	645	0.40
8c	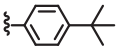	3176	0.34
8d	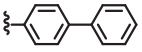	4883	0.30
8e	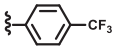	>31600	-
8f	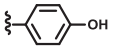	12760	0.35
8g	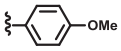	6076	0.36
8h	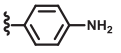	8477	0.37
5c	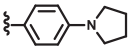	1814	0.34
8i	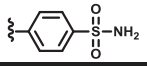	>31600	-

30K member hybrid fragment library, the informer library, which consisted of molecules that were > 200 MW and < 350 MW. By biasing the deck with larger fragments we hoped to increase of the possibility of a hit with < 250 μM potency in a high concentration screen.[8] Since G-protein coupled receptors still remain a challenge for biophysical fragment screening methods, we proposed that our hybrid-fragment library might prove productive in identifying novel chemical matter for GPCR targets.

Our work initiated with screening our hybrid fragment library at 100 μM in a cAMP assay, which led to the identification of 500 hits with inhibition of > 30% inhibition. A counter-screen of these 500 hits against a non-related GPCR (GPR74) resulted in 20 unique compounds. The compounds were purified and titrated in quadruplicate against NPBWR1 giving three compounds that showed dose-dependent inhibition. One of these hits was methylsulfone benzimidazole **1** (Fig. 1). Further follow-up of **1** by use of SAR-by-catalogue resulted in compound **2** with a 25-fold improvement in potency. Initial SAR of **2** quickly identified compound **3c** with a further 7-fold increase in potency. For the purpose of this article ligand efficiency (LE) index[9] and potency were used as guidelines for SAR optimization. The potency

Table 3
Exploration of the disubstituted and trisubstituted right-hand aryl ring.

cmpd	R	cAMP IC_{50} (nM)	LE
9a	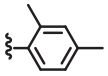	1544	0.40
9b	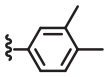	1384	0.40
9c	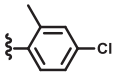	2486	0.38
9d	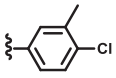	2286	0.39
9e	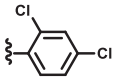	2879	0.38
9f	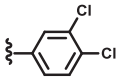	>31,600	-
9g	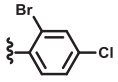	1755	0.40
9h	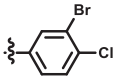	>31,600	-
9i	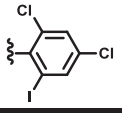	205	0.44

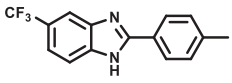

10

h cAMP IC_{50} = 791 nM
MW = 276
LE = 0.42

Fig. 2. In vitro potency of analog **10** at human NPBWR1.

Table 4
Exploration of heteroaromatic groups at the *para* position.

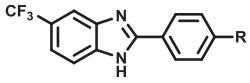

cmpd	R	cAMP IC_{50} (nM)	LE
13a		282	0.37
13b		1190	0.34
13c	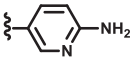	877	0.32
13d	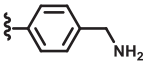	720	0.31
13e		996	0.34
13f		3082	0.32
13g		1465	0.32
13h		1197	0.29

described will be at the human receptor unless otherwise indicated.

Compound **3c** was chosen as a starting point to further optimize as it retained excellent LE (0.42). The systematic initial SAR focused on exploring the effect of a monosubstituted *ortho*, *meta*, and *para* right-hand aryl moiety by condensation of nitro phenylenediamine **7** with the appropriate benzaldehydes to afford corresponding benzimidazoles (Scheme 1, Table 1). Regardless of the electronic effect of the selected functional groups and without exception, *para* substituents (**3c**, **4c**, **5c**, **6c**) were the most potent.

Based on these data, we further investigated the SAR at the monosubstituted *para* position to improve potency of **3c** (Table 2). Extension of the alkyl chain from a methyl group of compound **3c** to a longer alkyl chain (**8a-b**) increased the potency by two-fold. Propyl compound **8b** was the most potent. The potency of **8b** increased 2-fold over **3c**, however this was at the cost of a decrease in LE. Substitution to bulkier *t*-butyl (**8c**) and phenyl (**8d**) groups further decreased the functional activity. Replacement of the methyl group of compound **3c** with a trifluoromethyl (**8e**) also proved detrimental to potency. Next, we

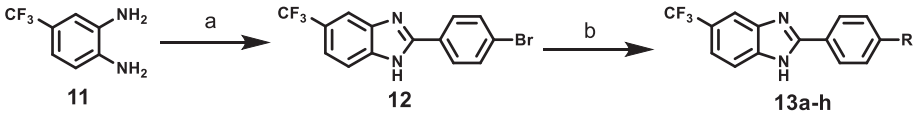

11 12 13a-h

Scheme 2. Reagents and conditions: (a) 1,4-benzoquinone, p-bromobenzaldehyde, 75 0C, 2 h; (b) Pd (PPh3)4, 1.0 M K2CO3, R-B(OH)2, 110 0C, 15 min.

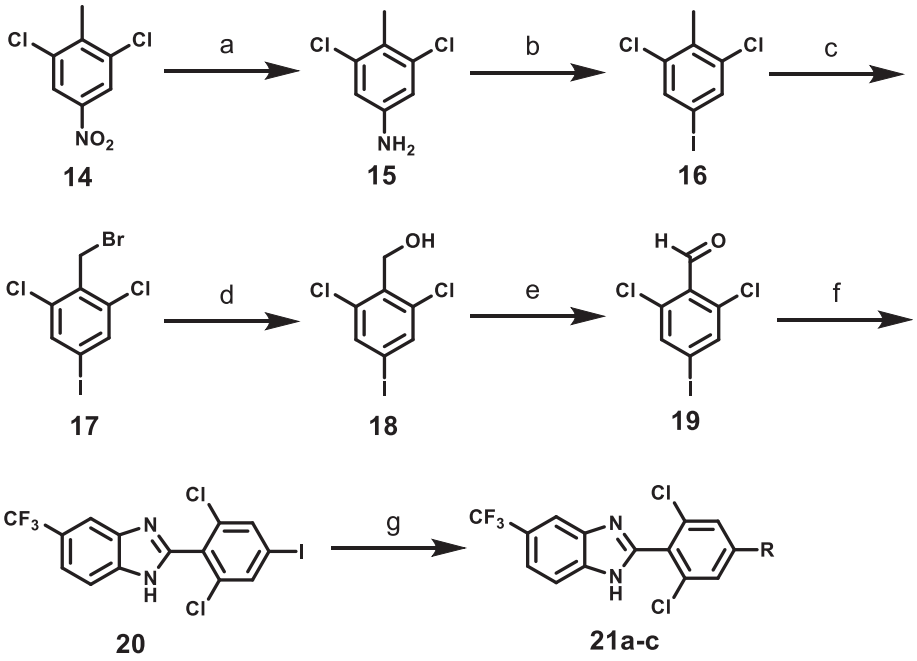

Scheme 3. Reagents and conditions: (a) $SnCl_2{\cdot}H_2O$, reflux, 2 h; (b) $NaNO_2$, KI, TsOH, 10 ^{0}C to rt, 1 h; (c) NBS, benzoyl peroxide, reflux, overnight; (d) i. KOAc, rt, overnight, ii. NaOH, reflux, 1 h; (e) Dess-Martin Periodinane, rt, 2 h; (f) 4-trifluorobenzene-1,2-diamine, 1,4 benzoquinone, 75 ^{0}C, overnight; (g) Pd $(PPh_3)_4$, R-$B(OH)_2$, 1.0 M K_2CO_3, 110 ^{0}C, 15 min.

Table 5
Trisubstituted aryl group with narrowly focused *p*-heteroaromatics for an additive effect in potency.

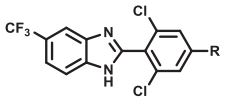

cmpd	R	cAMP IC_{50} (nM)	LE
21a		30	0.39
21b	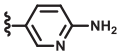	53	0.36
21c	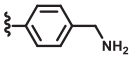	70	0.34

investigated substitution with polar substituents baring hydrogen bond donors and acceptors (**5c, 8f-i**). All resulted in a reduction in potency and LE.

To expand the SAR further, our efforts were directed towards exploring 2,4- (*ortho*, *para*), 3,4- (*meta*, *para*) disubstitution and subsequently 2,4,6-trisubstitution[10] on the distal aryl ring while maintaining methyl and chloro groups at the *para* position. Table 3 summarizes some of these combinations. Analogs with small substitution such as methyl (**9a-d**) were comparable to **3c** and **4c**, and there was no distinction in potency difference whether the methyl moiety was at the *ortho* or *meta* position. The presence of a chlorine and bromine atom at the *ortho* position (**9e**, **9g**) provided an additional small enhancement (1.5-fold) to the potency of **4c**. However, the substitution at the *meta* position (**9f**, **9h**) proved detrimental to potency, suggesting that 2,4-disubstitution on the aryl group was superior compared to its counterpart. Interestingly, introduction of another substituent at the 6 position, trisubstituted **9i**, resulted in a significant improvement in both potency (~13-fold) and LE relative to **4c** (0.44 vs 0.40).

Concurrent with exploring the SAR on the nitro containing benzimidazole series, we aimed to replace the nitro moiety due to its potential inherent metabolic liabilities in vivo. Early in our work we discovered that trifluromethyl containing benzimidazole **10** had a two-fold increase in potency over **3c** (Fig. 2).

We further studied the scope of the SAR by examining heteroaromatic groups at the *para* substitution of the phenyl group of compound **10**. As illustrated in Scheme 2, trifluoromethyl phenylenediamine **11** was converted to trifluoromethyl benzimidazole **12** by condensation with *p*-bromobenzaldehyde. Compound **12** served as an ideal key intermediate to quickly access analogs via Suzuki cross-coupling.

Table 4 shows various heteroaromatics that were examined. Pyrazole containing compound **13a** was 3-fold more potent than the parent compound **10**. Additionally, other heteroaromatic containing compounds (**13b-e**) were well tolerated. However, triazole analog **13f** was 4-fold less potent than **10**. We then further functionalized the pyrazole moiety (**13g-h**). Both compounds resulted in potency loss.

With the discovery of productive SAR on the right-hand side, we investigated whether the potency gains from trisubstituted and *para* heteroaromatic analogs would be additive. Aldehyde **19** was quickly synthesized in a linear fashion (Scheme 3).[11] Aryl nitro **14** was reduced with tin (II) chloride to give aniline **15**, which underwent Sandmeyer chemistry to furnish aryl iodide **16**. Bromination of the methyl group

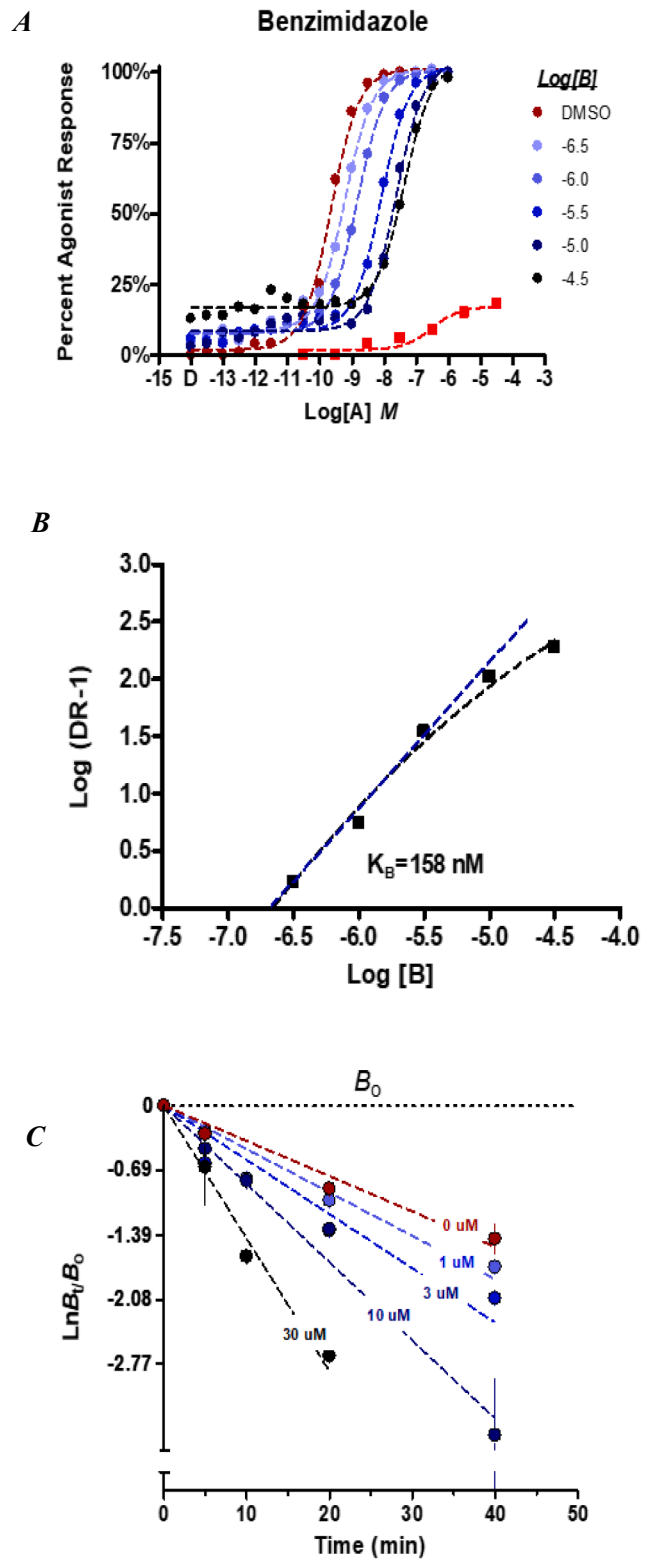

Fig. 3. Using compound 21a as a representative in the benzimidazole class, A. Agonist titration curves ([A] = concentration of NPW, [B] = concentration of 21a), B. Schild plot analysis, C. Off-rate kinetics experiment.

with NBS and benzoyl peroxide afforded benzyl bromide **17**, which was then followed by displacement of the bromide with potassium acetate and a subsequent treatment with sodium hydroxide to give benzyl alcohol **18**. Oxidation of **18** with Dess-Martin led to the formation of benzaldehyde **19**, which was then condensed with trifluoromethyl phenylenediamine **11** to yield benzimidazole **20**. Suzuki coupling of iodide with tetrakis(triphenylphosphine)palladium furnished final compound **21**.

As shown in Table 5, the hybrid compounds (**21a-c**) had a significant improvement in potency, with IC_{50} values in the nanomolar range. Pyrazole containing compound **21a** resulted in the most potent analog. Indeed, by comparing **13a** and **21a**, analog **21a** exhibited both potency (~10 fold) and LE (0.37 vs. 0.39) gains.

To obtain a more rigorous estimate of antagonist potency, we attempted to characterize the pK_B of benzimidazole representative compound **21a** by Schild analysis. As demonstrated in Fig. 3A, and consistent with inhibition of agonist activity in our cAMP assay, titration of compound **21a** resulted in a parallel rightward shift of equipotent agonist doses. Unexpectedly however, the dextral displacement of agonist dose response curves elicited by compound **21a** appeared to be saturable and, indeed, the Schild replot of the data (Fig. 3B) is curvilinear. Moreover, compound **21a** appeared to dose-dependently inhibit forskolin-stimulated cAMP accumulation in cells expressing GPR7 in its own right, both in the context of cross-titration and when independently tested in the agonist mode of the assay (red trace, Fig. 3A). That is, compound **21a** appears to act as a partial agonist of GPR7. To further investigate the mechanism of inhibition of compound **21a**, we turned to a homogeneous, real-time SPA binding assay to examine the off-rate kinetics of 125I-hNPW23 both in the presence and absence of compound **21a** (Fig. 3C). Toward this end, membranes were prepared from CHO cells recombinantly overexpressing GPR7, and pre-equilibrated with a saturating concentration of 125I-hNPW23. Dissociation of the pre-bound radioiodinated agonist was then initiated by dilution into a large volume of binding buffer containing 0–30 μM compound **21a**, and revealed that the k_{off} of 125I-hNPW23 is dose dependently accelerated by **21a**. Taken collectively, these data are inconsistent with neutral, strictly competitive antagonism of NPW23 at GPR7 and, rather, suggest that compound **21a** may act as an antagonist of GRP7, at least in part, by allosterically reducing the affinity of hNPW23 for its cognate receptor. The Schild replot for such data is linear.

In summary, a fragment-based screen was utilized to find a novel benzimidazole series as GPR7 antagonists. Potency and LE index were used as guidelines to optimize the series. As indicated in Scheme 4, we have demonstrated the ability to advance a weak binder and low LE of methylsulfone benzimidazole **1**. The first success came from the discovery of nitro benzimidazole **2** and eventually trifluoromethyl benzimidazole **22**, which enhanced the potency to a low micromolar range. Subsequent optimization at the *para* position with pyrazole followed by an additive effect at the 2,6-position produced notable compound **21a** with a 6,700-fold increase in potency and a significant gain in LE. Additionally to have a deeper understanding of the molecular interaction between the benzimidazole class and the GPR7 receptor, we conducted Schild plot analysis and off-rate kinetics experiments using compound **21a** to represent the benzimidazole series. Based on Schild analysis, the graph diverged from linearity. As the concentration of the compound increased, the graph would eventually plateau, indicating that the series did not exhibit competitive antagonism. Furthermore by examining the off-rate kinetics study, it showed that the series accelerated the off-rate between the indigenous ligand (NPW) and the GPR7 receptor as the concentration of **21a** increased.

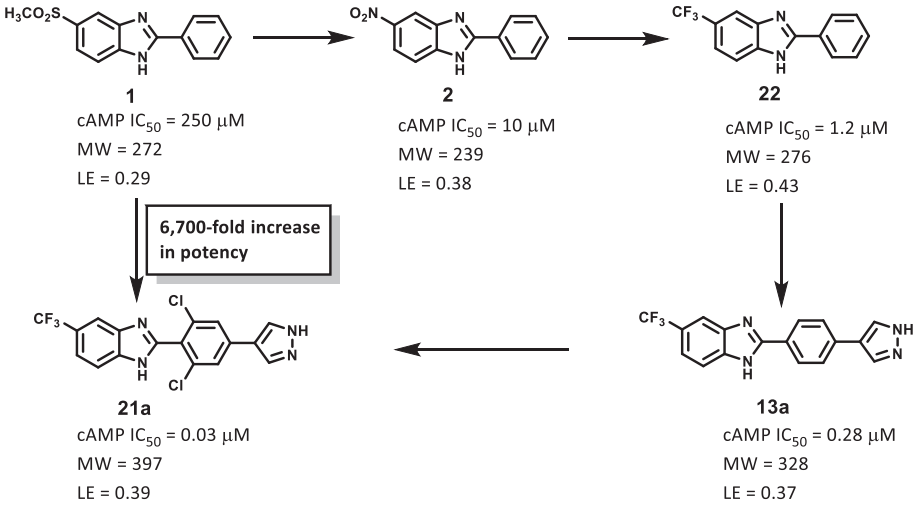

Scheme 4. From hit **1** to lead **21a**.

Declaration of Competing Interest

The authors declare that they have no known competing financial interests or personal relationships that could have appeared to influence the work reported in this paper.

Appendix A. Supplementary data

Supplementary data to this article can be found online at https://doi.org/10.1016/j.bmcl.2020.127510.

References

1. (a) Fujii R, Yoshida H, Fukusumi S, et al. *J. Biol. Chem.* 2002;277:34010
   (b) Shimomura Y, Harada M, Goto M, et al. *J. Biol. Chem.* 2002;277:35826
   (c) Brezillon S, Lannoy V, Franssen JD, et al. *J. Biol. Chem.* 2003;278:776
   (d) Tanaka H, Yoshida T, Miyamoto N, et al. *Proc. Natl. Acad. Sci. U.S.A.* 2003;100:6251.
2. Jackson VR, Lin SH, Wang Z, Nothacker HP, Civelli O. *J. Comp. Neurol.* 2006;497:367.
3. Hondo M, Ishii M, Sakurai T. *Results Probl. Cell. Differ.* 2008;46:239.
4. Ishii M, Fei H, Friedman JM. *Proc. Natl. Acad. Sci. U.S.A.* 2003;100:10540.
5. Romero FA, Hastings NB, Moningka R, et al. *Bioorg. Med. Chem. Lett.* 2012;22:1014.
6. (a) Urbano M, Guerrero M, Zhao J, et al. *Bioorg. Med. Chem. Lett.* 2012;22:7135
   (b) Guerrero M, Urbano M, Schaeffer M-T, Brown S, Rosen H, Roberts E. *Bioorg. Med. Chem. Lett.* 2013;23:614.
7. Rees DC, Congreve M, Murray CW, Carr R. *Nat. Rev. Drug Discov.* 2004;3:660.
8. Lan P, Romero FA, Wodka D, et al. *J. Med. Chem.* 2017;60:9040.
9. For ligand efficiency index concept and calculation: (a) Kuntz, I. D.; Chen, K.; Sharp, K. A.; Kollman, P. A. Proc. Natl. Acad. Sci. U.S.A. 1999, 96, 9997; (b) Hopkins, A. L.; Groom, C. R.; Alex, A. Drug Discovery Today. 2004, 9, 430; (c) Abadzapatero, C.; Metz, J. Drug Discovery Today. 2005, 10, 464; (d) Leeson, P. D.; Springthorpe, B. Nat. Rev. Drug Discov. 2007, 6, 881; (e) Keseru, G. M.; Makara, G. M. Nat. Rev. Drug Discov. 2009, 8, 203.
10. Numbering system on the right-hand aryl group was depicted in figure 1 compound 1.
11. Representative experimental procedure (compound 21a): A mixture of 1,3-dichloro-2-methyl-5-nitrobenzene (3.00 g, 14.56 mmol) 14 and tin(II) chloride dihydrate (13.14 g, 58.2 mmol) in ethanol (48.5 mL) was heated under reflux for 2 h. The reaction mixture was allowed to cool to rt, and quenched carefully with water and sat. aqueous solution of NaHCO3 until slightly basic. The thick slurry mixture was filtered through a pad of celite, and the filtrate was extracted with EtOAc (3x). The combined extracts were dried over Na2SO4, filtered, and concentrated under vacuum. The crude residue was purified by silica gel chromatography, eluting with 0-20% EtOAc/hexanes to give 3,5-dichloro-4-methylaniline 15 (1.13 g, 44%). LCMS: m/z 176 [M+H]+. To a solution of tosic acid (3.66 g, 19.26 mmol) in acetonitrile (25.7 mL) was added 3,5-dichloro-4-methylaniline 15 (1.13 g, 6.42 mmol). The resulting suspension of amine salt was cooled to 10-15 °C, and to this was added a solution of sodium nitrite (0.886 g, 12.84 mmol) and potassium iodide (2.66 g, 16.05 mmol) in water (4.0 mL). The reaction mixture was stirred for 10 min, then allowed to come to rt and stirred for 1 h. Water was then added followed by 1.0 M aqueous NaHCO3 and Na2S2O3. The mixture was extracted with DCM (3x), and the combined organic layers were dried over Na2SO4, filtered, and concentrated under vacuum. The crude residue was purified by silica gel chromatography, eluting with 0-10% EtOAc/hexanes to give 2,6-dichloro-4-iodotoluene 16 (1.23 g, 67%) as a pale brown solid. 1H NMR (d6-DMSO, 500 MHz): δ 7.77 (s, 2H), 2.21 (s, 3H). To a solution of 1,3-dichloro-4-iodotoluene 16 (1.23 g, 4.29 mmol) in CCl4 (14.29 mL) was added NBS (1.907 g, 10.72 mmol) followed by benzoyl peroxide (0.052 g, 0.214 mmol). The reaction mixture was heated at reflux overnight, then cooled to rt, and filtered through a pad of celite. The solvent was removed under vacuum, and the residue was purified by silica gel chromatogarphy, eluting with 0-5% EtOAc/hexanes to afford 5-iodo-2-(bromomethyl)-1,3-dichlorobenzene 17 (1.54 g, 98%) as an orange crystal. 1H NMR (CDCl3, 500 MHz): δ 7.67 (s, 2H), 4.67 (s, 2H). To a solution of 5-iodo-2-(bromomethyl)-1,3-dichlorobenzene 17 (700 mg, 1.914 mmol) in acetonitrile (9.50 mL) was added potassium acetate (751 mg, 7.65 mmol). The reaction was stirred at rt overnight. The solid was then filtered, and the filtrate was evaporated under vacuum. The resulting residue was dissolved in EtOH (10 mL), and treated with 5.0 M aqueous sodium hydroxide (765 μL, 3.83 mmol). The reaction mixture was heated at reflux for 1 h, then cooled to rt, and extracted with EtOAc (3x). The combined extracts were dried over Na2SO4, filtered, and concentrated under vacuum to yield crude (2,6-dichloro-4-iodophenyl)methanol 18 (547 mg, 94%) as an orange solid. (2,6-Dichloro-4-iodophenyl)methanol 18 (547 mg, 1.806 mmol) was dissolved in dichloromethane (18.0 mL), and Dess-Martin Periodinane (1149 mg, 2.71 mmol) was added in one portion. The reaction mixture was stirred at rt for 2 h before the solvent was evaporated under vacuum. The crude residue was purified by silica gel chromatography, eluting with 0-15% EtOAc/hexanes to afford 2,6-dichloro-4-iodobenzaldehyde 19 (443 mg, 82%) as a pale-orange solid. 1H NMR (CDCl3, 500 MHz): δ 10.4 (s, 1H), 7.76 (s, 2H). Trifluoromethyl phenylenediamine 11 (235 mg, 1.334 mmol), 1,4-benzoquinone (159 mg, 1.468 mmol), and 2,6-dichloro-4-iodobenzaldehyde 19 (442 mg, 1.468 mmol) were dissolved in Ethanol (8894 μL), and the reaction mixture was heated to 75 °C overnight. The reaction mixture was then allowed to cool to rt, and the solvent was evaporated under vacuum. The crude mixture was purified by silica gel chromatography, eluting with 0-25% EtOAc/hexanes to afford 2-(2,6-dichloro-4-iodophenyl)-5-(trifluoromethyl)-1H-benzimidazole 20 (449 mg, 74%) as a brownish gray solid. LCMS: m/z 457 [M+H]+. 2-(2,6-Dichloro-4-iodophenyl)-5-(trifluoromethyl)-1H-benzimidazole 20 (30 mg, 0.066 mmol), palladium tetrakis (7.59 mg, 6.56 μmol), 1.0 M aqueous potassium carbonate (197 μL, 0.197 mmol), and 4-pyrazoleboronic acid pinacol ester (5.88 mg, 0.131 mmol) were mixed in dioxane (656 μL). The resulting mixture was heated to 110 °C for 15 min under microwave irradiation. The solvent was then evaporated under vacuum, and the crude mixture was purified by RP HPLC to give 2-[2,6-dichloro-4-(1H-pyrazol-4-yl)phenyl]-5-(trifluoromethyl)-1H-benzimidazole 21a (9.10 mg, 34%). 1H NMR (500 MHz, Methanol-d4) δ 8.22 (s, 1H), 8.06 (s, 1H), 7.93 (s, 1H), 7.89 (d, J = 8.5 Hz, 1H), 7.71 (dd, J = 8.6, 1.4 Hz, 1H), 7.70 – 7.64 (m, 1H), 7.61 – 7.56 (m, 1H). LCMS: m/z 397 [M+H]+.